ACS APPLIED MATERIALS & INTERFACES

Research Article

www.acsami.org

Charge Generation Layers for Solution Processed Tandem Organic Light Emitting Diodes with Regular Device Architecture

Stefan Höfle,*[,†,▽] Christoph Bernhard,[†,▽] Michael Bruns,[§,∥] Christian Kübel,[‡,∥] Torsten Scherer,[‡,∥] Uli Lemmer,[†,⊥] and Alexander Colsmann*[,†]

[†]Light Technology Institute, Karlsruhe Institute of Technology (KIT), Engesserstrasse 13, 76131 Karlsruhe, Germany

[‡]Institute of Nanotechnology, Karlsruhe Institute of Technology (KIT), Hermann-von-Helmholtz-Platz 1, 76344 Eggenstein-Leopoldshafen, Germany

[§]Institute for Applied Materials, Karlsruhe Institute of Technology (KIT), Hermann-von-Helmholtz-Platz 1, 76344 Eggenstein-Leopoldshafen, Germany

[∥]Karlsruhe Nano Micro Facility (KNMF), Karlsruhe Institute of Technology (KIT), Hermann-von-Helmholtz-Platz 1, 76344 Eggenstein-Leopoldshafen, Germany

[⊥]Institute for Microstructure Technology, Karlsruhe Institute of Technology (KIT), Hermann-von-Helmholtz-Platz 1, 76344 Eggenstein-Leopoldshafen, Germany

ABSTRACT: Tandem organic light emitting diodes (OLEDs) utilizing fluorescent polymers in both sub-OLEDs and a regular device architecture were fabricated from solution, and their structure and performance characterized. The charge carrier generation layer comprised a zinc oxide layer, modified by a polyethylenimine interface dipole, for electron injection and either MoO_3, WO_3, or VO_x for hole injection into the adjacent sub-OLEDs. ToF-SIMS investigations and STEM-EDX mapping verified the distinct functional layers throughout the layer stack. At a given device current density, the current efficiencies of both sub-OLEDs add up to a maximum of 25 cd/A, indicating a properly working tandem OLED.

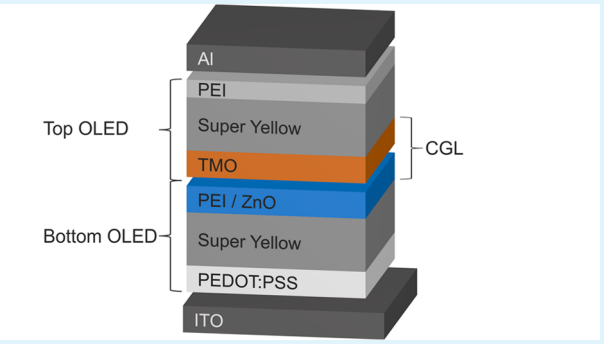

KEYWORDS: *organic light emitting diode, solution processing, charge generation layer, tandem OLED, stacked OLED, multiphoton emission*

INTRODUCTION

Organic light emitting diodes (OLEDs) have been thoroughly investigated due to their beneficial optoelectronic properties for display applications or general lighting.[1−4] For the fabrication of OLEDs on an industrial scale, the deposition of organic semiconductors by either vacuum evaporation or solution deposition (such as printing or coating) has been considered. Whereas thermal evaporation enables high device performance by stacking an arbitrary number of functional layers for improved charge carrier transport, the fabrication of advanced solution processed multilayer devices remains challenging due to solvent limitations.

After OLED efficiencies have been improved well beyond 100 lm/W over the last couple of years, future research will have to focus on the device lifetime to make the OLED technology competitive to other light sources for general lighting.[5,6] OLED degradation and subsequent failure is often caused by high device currents.[7,8] A promising concept to reduce the device current while preserving the device luminance is the tandem architecture, where two (or more) OLEDs are stacked on top of each other. In this architecture, ideally, multiple photons are emitted from each injected electron−hole pair, thereby reducing the device stress. In order to stack two OLEDs, a monolithic interconnecting unit, commonly referred to as the charge carrier generation layer (CGL), is required which ensures efficient charge carrier injection into the adjacent emission layers. Common CGLs incorporate a high- and a low-work function material such as electrically doped organic semiconductors, ultrathin metal layers, transparent conductive oxides, or transition metal oxides (TMOs), typically all deposited by vacuum evaporation.[5,9−15] For future OLED fabrication, however, printing is often considered as a low-cost and high-throughput manufacturing alternative. The design and fabrication of efficient CGLs is key for high-performance tandem OLEDs, in particular, when only solution processes are considered. Recently, we reported on solution processed organic tandem OLEDs with an inverted architecture (top anode, bottom cathode), where we employed CGLs comprising high-work function tungsten oxide (WO_3), poly(3,4-ethylenedioxythiophene):poly(styrenesulfonate) (PE-

Received: January 29, 2015
Accepted: April 2, 2015
Published: April 2, 2015

DOI: 10.1021/acsami.5b00883
ACS Appl. Mater. Interfaces 2015, 7, 8132−8137

DOT:PSS) as solvent barrier and moderate work function zinc oxide (ZnO).[16] Unfortunately, ZnO/PEDOT:PSS CGLs cannot be used in regular device architectures (top cathode, bottom anode) where the acidic PEDOT:PSS would inevitably dissolve the underlying ZnO layer, with the often observed device lifetime reduction upon PEDOT:PSS utilization being another problem. Therefore, all-solution processed tandem OLEDs with regular architecture will require a different design and in particular a different set of functional materials to form the CGLs. So far, only partly solution processed CGLs with additional vacuum evaporated layers have been applied in tandem OLEDs with regular device architecture.[17−19] With a work function of $\Phi_a \approx 4.1$ eV,[20,21] ZnO is one of the few solution processable materials that can be employed for electron injection into OLEDs if it is modified by interface dipoles.[22−24] In the closely related field of organic photovoltaics, precursor based, solution processable, high-work function TMOs such as WO_3, molybdenum oxide (MoO_3), or vanadium pentoxide (V_2O_5) were extensively analyzed and used in recombination zones of tandem solar cells.[25−33] Although solution processable TMOs are commonly used in organic photovoltaic devices, their use for OLED has hardly been investigated.[31,34,35]

In this paper we present CGLs comprising ZnO and one of the high-work function TMOs WO_3, MoO_3, or V_2O_5 to enable solution processing of efficient singlet-emitting polymer tandem OLEDs with regular device architecture.

EXPERIMENTAL SECTION

All tandem OLEDs were fabricated on indium tin oxide (ITO) coated glass substrates ($R_\square \approx 13\ \Omega/\square$) that had been structured with hydrochloric acid. The substrates were cleaned with acetone and isopropanol in an ultrasonic bath (15 min). Afterward the substrates were exposed to an oxygen plasma (2 min) in order to remove organic residues and to polarize the ITO surface for better adhesion. Unless otherwise noted, the deposition processes were carried out in inert atmosphere.

PEDOT:PSS (Heraeus Clevios VP AI 4083) was diluted by water (1:1), spin-cast (4000 rpm, 25 s, 20 nm) and annealed (120 °C, 10 min) to remove water residuals. A fluorescent Super Yellow emission layer (Merck) was spin-cast from toluene solution (4 g/L, 1000 rpm, 60 s, 70 nm). For the bottom OLED, Super Yellow was annealed at 205 °C to prevent dissolving upon subsequent deposition of additional layers.[36] To ensure an efficient electron injection, a PEI layer was spin-cast from isopropanol solution (3.9 g/L, 5000 rpm, 50 s) adapting the process suggested by Zhou et al.[37] Afterward, the samples were annealed in ambient conditions (10 min, 100 °C). The deposition of the ZnO layer (30 nm) was adapted from De Bruyn et al.[20] Therefore, zinc acetylacetonate hydrate ($Zn(acac)_2$, Sigma-Aldrich) was dissolved in ethanol (20 g/L) and stirred (24 h, T = 50 °C). The solution was filtered using a 0.2 μm PTFE filter to remove precursor aggregates. The $Zn(acac)_2$ solution was spin-cast (2000 rpm, 45 s) and subsequently annealed (30 s, 120 °C) to form ZnO in ambient conditions. Then, by precursor deposition, hydrolysis and condensation either the WO_3, the MoO_3 or the VO_x TMO was applied. The tungsten(VI)ethoxide ($W(OEt)_6$) or the molybdenum(V)ethoxide ($Mo(OEt)_5$) precursor solutions (ABCR Dr. Braunagel GmbH & Co. KG) were diluted in isopropanol (1:80 or 1:120 by volume, respectively) and spin-cast (4000 rpm, 30 s, 15 nm). The $W(OEt)_6$ layer was converted to WO_3 at room temperature. $Mo(OEt)_5$ was annealed in air at 150 °C for 10 min to form MoO_3 according to the processes described in our previous publications.[34,35] Both processes had been proven to yield WO_3 and MoO_3 with proper stoichiometry before. The vanadium oxide (VO_x) layers were applied by spin coating a vanadium triisoproxide oxide precursor (4000 rpm, 30 s, 15 nm) from isopropanol solution (1:100 by volume) and subsequently annealed (120 °C, 1 min) in ambient conditions.[32,38] For the fabrication of the top OLED, the emitter polymer (without annealing) and the PEI deposition processes were repeated. For the counter electrode, aluminum was thermally evaporated (200 nm).

The OLED current density−voltage (J−V) characteristics were recorded with a source measurement unit (Keithley 238). The device luminance was calculated from the emission spectrum. The spectrometer had been calibrated with a secondary standard halogen lamp (Philips FEL-1000W). Current efficiencies (in cd/A) were calculated from the electrical and optical properties assuming Lambertian light distribution.

Time-of-flight secondary ion mass spectrometry (ToF-SIMS) was performed on a TOF.SIMS^5 instrument (ION-TOF GmbH, Münster, Germany), equipped with a Bismuth (Bi) cluster liquid metal primary ion source and a nonlinear time-of-flight analyzer. The Bi source was operated in the "bunched" mode providing 0.7 ns Bi_1^+ ion pulses at 25 keV energy and a lateral resolution of approximately 4 μm. Negative polarity spectra were calibrated on the C^-, C_2^-, and C_3^- peaks. Sputter depth profiles were performed using a 1 keV Cs^+ ion beam and a raster size of 400 × 400 μm^2. The analyzed area was 100 × 100 μm^2 in the center of the sputter crater.

Transmission electron microscopy (TEM) analysis was performed using an aberration corrected (image) Titan 80-300 (FEI Company, Portland, USA), operated at an acceleration voltage of 300 kV and equipped with an S-UTW EDX detector (EDAX). Images were recorded with a high angle annular dark-field detector (HAADF) in scanning transmission electron microscopy (STEM) mode with a nominal spot size of 0.14 nm. Initial imaging was performed under strict low-dose conditions with a total dose of about 1 e/Å^2 for the first image. As no morphology changes were visible over an extended image series, the final images were acquired close to standard imaging conditions. STEM-EDX elemental maps were obtained with a nominal spot size of 0.5 nm.

TEM cross-section samples of the OLEDs were prepared by in situ lift-out using a Strata 400 S focused ion beam (FIB) system (FEI Company, Portland, USA). Initial preparation was performed using 30 kV Ga^+ ions and final polishing at 5 and 2 kV. SEM imaging at 1 kV was limited to a minimum to exclude beam damage of the OLEDs during preparation.

RESULTS AND DISCUSSION

The regular tandem OLEDs were fabricated according to the device architecture depicted in Figure 1 incorporating CGLs from ZnO and a high-work function TMO. Both ZnO and the TMO are n-doped and exhibit a significant difference of work functions, accounting for a proper alignment of the electron and hole transport energy levels in the bottom and the top OLEDs, respectively. Charge generation, however, takes place at the TMO/organic interface with holes being injected into

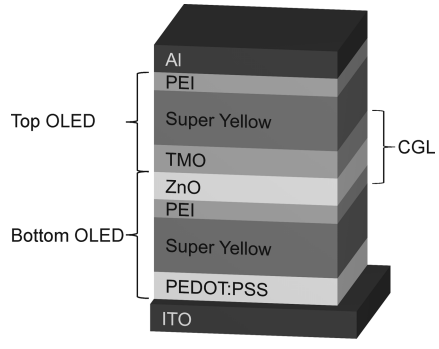

Figure 1. Device architecture of the regular tandem OLED comprising two Super Yellow emission layers and a ZnO/TMO charge generation layer. The TMO layers were implemented by solution processing of either WO_3, MoO_3, or VO_x.

DOI: 10.1021/acsami.5b00883
ACS Appl. Mater. Interfaces 2015, 7, 8132−8137

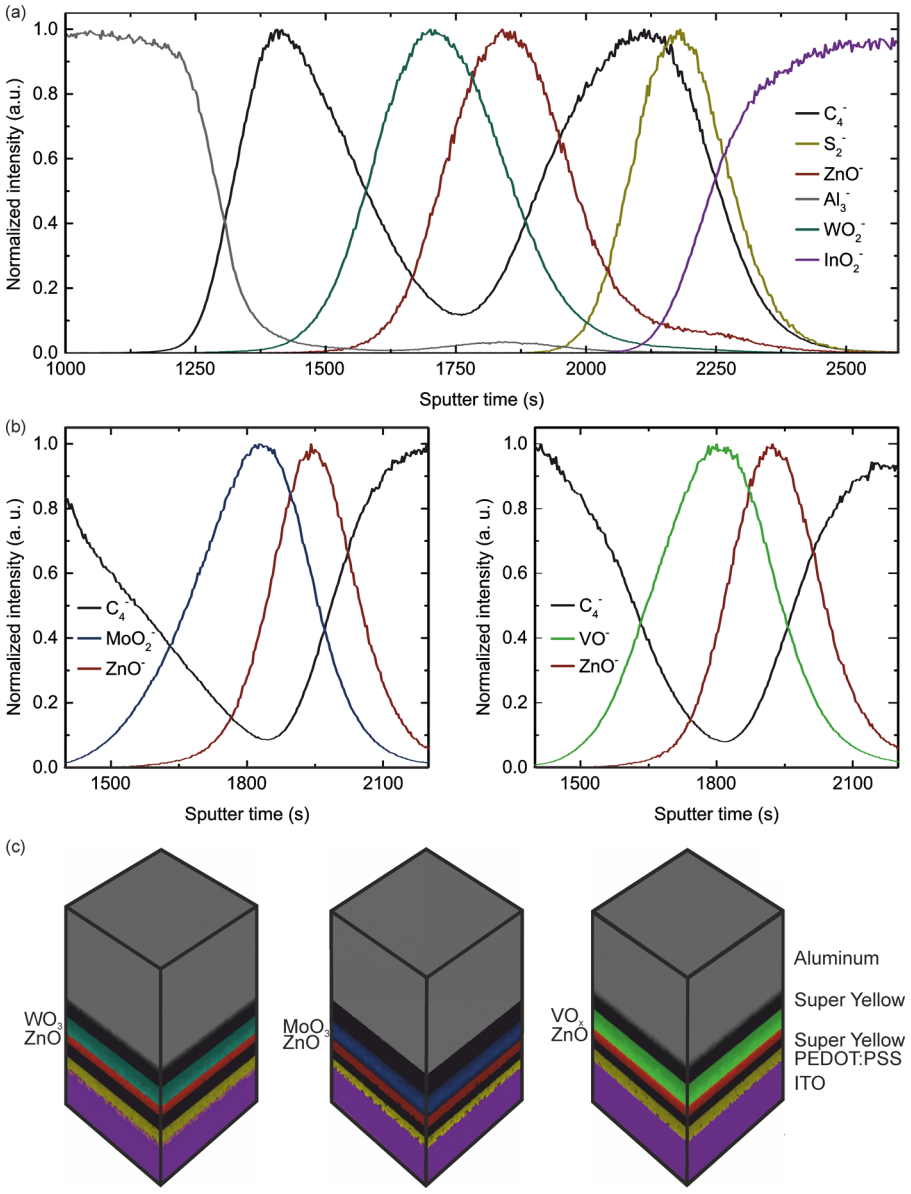

Figure 2. (a) Normalized ToF-SIMS signals of the characteristic fragments Al_3^- (Al), C_4^- (Super Yellow, PEI), WO_2^- (WO_3), ZnO^- (ZnO), S_2^- (PEDOT:PSS), and InO_2^- (ITO) versus sputter time of a typical polymer tandem OLED. The distinct profiles indicate good definition of the layers and hence a successful implementation of the solution processed multilayer stack. (b and c) Normalized ToF-SIMS signals of the CGLs comprising ZnO/MoO_3 or ZnO/VO_x. The data of the other functional layers match the data in part a. (d) Reconstructed 3D visualization of the OLED stacks based on the respective analyzed 100 × 100 μm^2 areas.

Super Yellow and electrons being injected into the TMO.[9] In solution processed multilayer OLEDs, intermixing of adjacent layers during layer deposition is a major threat to the device performance and can ultimately lead to device failure. Especially in tandem OLEDs, accurate multilayer stacking is necessary to ensure efficient charge carrier generation within the CGLs and charge carrier injection into the emission layers. Hence, before assessing the optoelectronic device properties, we performed ToF-SIMS and STEM-EDX measurements on the tandem OLEDs to verify a successful implementation of the solution processed multilayer stack. The intensities of the ToF-SIMS signals from the relevant molecular fragments versus the cesium ion sputter time are shown in Figure 2a for the OLED that employs a CGL from ZnO and WO_3. The signals monitor the layer sequence within the OLED from the aluminum counter electrode to the bottom ITO anode: the aluminum cathode (Al_3^-) is followed by a carbon signal (C_4^-) from the Super Yellow and PEI. The subsequent CGL is identified by a WO_2^- signal related to the WO_3 layer and a zinc oxide signal (ZnO^-). Further in sputter time, the bottom OLED is represented by another carbon signal for the Super Yellow and PEI layers. A sulfur signal (S_2^-) tracks the PEDOT:PSS hole injection layer. Finally, we observe the ITO anode (InO_2^-) signal. The distinct signals of the various functional layers indicate a well-defined layer sequence throughout the device with limited overlap between the ZnO^- and WO_2^- signals. We find the same well-defined layers when replacing WO_3 by MoO_3 or VO_x, which provides further degrees of freedom for the device architecture design. The respective ToF-SIMS profiles of the ZnO/MoO_3 and ZnO/VO_x CGLs are depicted in Figures 2b and 2c, clearly distinguishing the ZnO and MoO_3 or ZnO and VO_x layers, respectively. Again, the CGL is framed by the carbon signal

DOI: 10.1021/acsami.5b00883
ACS Appl. Mater. Interfaces 2015, 7, 8132−8137

from the Super Yellow and PEI layers. The reconstructed device architectures based on the data gained from the ToF-SIMS measurements in Figure 2d illustrate the very good layer definition. The ToF-SIMS analysis was confirmed by HAADF-STEM and STEM-EDX analysis of the ZnO/WO_3 device (Figure 3). The HAADF-STEM images in Figure 3a are in

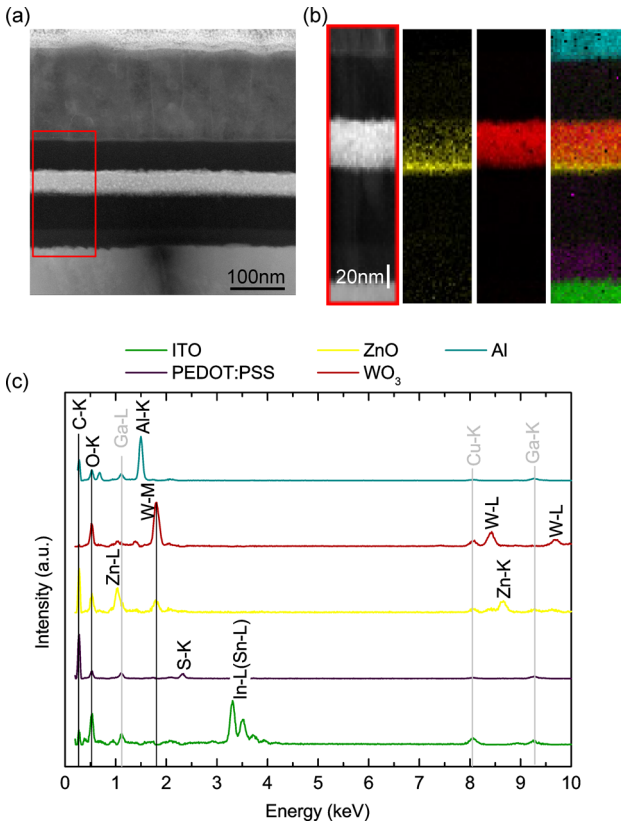

Figure 3. (a) HAADF-STEM cross section image of a typical device. (b) The HAADF-STEM reference image and the corresponding Multivariate EDX analysis of the tandem OLED comprising the ZnO/WO_3 CGL reveal the characteristic elements within the tandem device. Spatially resolved EDX mapping of the different elements shows good definition of the layers. (c) EDX spectra corresponding to the different components detected by Multivariate analysis. Ga- and Cu- signals originate from the FIB preparation and the TEM Grid.

good agreement with the nominal device architecture depicted in Figure 1 consisting of the ITO substrate followed by the ~32 nm PEDOT:PSS layer, the ~60 nm Super Yellow/PEI layer, the ~40 nm CGL, the second ~60 nm Super Yellow and PEI layer, and the Al top contact. All layers are very well-defined with low surface roughness. The STEM-EDX analysis further reveals the layer structure based on the characteristic elements in each layer depicted after Multivariate statistical analysis in Figure 3b. In particular, the STEM-EDX analysis enables a clear separation between the ZnO and WO_3 in the CGL and shows that ZnO is dominant in the bottom ~10 nm of the CGL as well as some ZnO intermixing with the WO_3 layer above in agreement with the ToF-SIMS profiles, which we attribute to the rough ZnO surface (R_q = 10.3 nm from AFM measurements) and consequently to the penetration of the WO_3 layer by ZnO domains.

After probing the definition of the layer stack, we investigated the optoelectronic properties of the tandem OLEDs. Besides the tandem devices, for reference, we built single emission layer OLEDs. In order to accurately resemble the sub-OLEDs, we incorporated the PEI and ZnO layers for electron injection into the reference bottom OLED and the TMO layer for hole injection into the reference top OLED. Accordingly, the reference bottom OLED utilized an ITO/PEDOT:PSS/Super Yellow/PEI/ZnO/Al architecture, whereas the reference top OLED utilized an ITO/TMO/Super Yellow/PEI/Al architecture. Hence, the reference bottom OLED is the same for all three tandem architectures. Comparing the reference devices, we observed an overall better performance of the top OLEDs compared to the bottom OLED which can be attributed to the temperature treatment of the bottom Super Yellow layer at 205 °C, which is known to lower the device performance.[36] Figure 4 shows the optoelectronic characteristics of the reference OLEDs and the corresponding tandem OLEDs. The $J-V$ curves are depicted in Figure 4a. For a given device current density, the driving voltages of the reference top and bottom OLEDs add up to the driving voltage of the tandem device, indicating an electrically properly working tandem OLED. Since the charges have to pass through two OLEDs, we expect an enhanced light emission versus device current density in the tandem OLED. This prediction is confirmed in Figure 4b, for all three CGLs. In the current density regime below 30 mA/cm^2, the luminances of the reference bottom and top OLEDs nicely add up to the luminances of the tandem OLEDs. For higher current densities the luminance of the tandem devices is somewhat lower than the sum of the two reference OLEDs. This deviation may result from the onset of an unbalanced electron−hole injection leading to a reduced current efficiency. This might be related to the current density dependent trap-related tunneling mechanisms in the CGL as discussed by Qi et al.[11,39] At a given luminance, the current efficiencies of the tandem devices in Figure 4c match the sum of the current efficiencies of the reference bottom and top devices. For example, in the device with a ZnO/WO_3 CGL, the current efficiency of about 25 cd/A matches the sum of 10 cd/A for the bottom and 15 cd/A for the top reference all over the luminance range that is commonly considered for general lighting, that is, between 1000 cd/m^2 and 8000 cd/m^2. Likewise, the power efficiency of the tandem device matches about the power efficiency of the reference device (Figure 4d). Both indicate an excellent and balanced charge carrier injection from the electrodes and the intermediate CGL.

We note, that in thin-film devices, cavity effects may play a role and influence the emission of OLEDs. A preliminary comparison of the emission spectra shows equal emission profiles, indicating a negligible impact of cavity effects on the device performance and emission.

CONCLUSION

We have investigated solution processed fluorescent tandem OLEDs with regular device architecture. In order to ensure proper electron injection into the bottom OLED, a combination of ZnO and PEI was incorporated into the CGL. For hole injection, high-work function TMOs (WO_3, MoO_3, and VO_x) were used. Current efficiencies up to 25 cd/A were reached in the tandem OLEDs. Further investigations will aim at the implementation of complementary emissive layers (such as orange and blue emitting polymers) to generate white light for general lighting. In future tandem OLEDs, triplet-emitting dyes may lead to enhanced device performances. The applied solution processes aim at future upscaling of the

DOI: 10.1021/acsami.5b00883
ACS Appl. Mater. Interfaces 2015, 7, 8132−8137

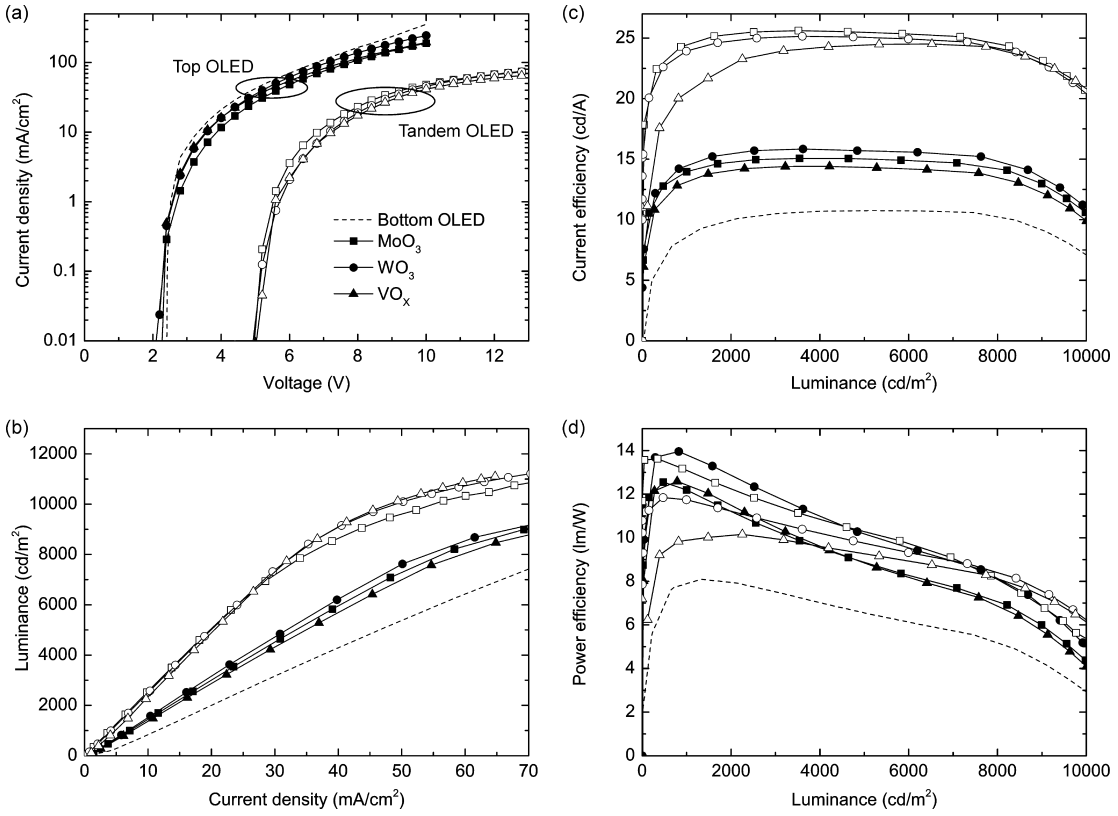

Figure 4. Optoelectronic properties of typical regular polymer tandem OLEDs comprising various TMOs as well as the top and bottom reference OLEDs. (a) *J*−*V* curves, (b) device luminances, (c) current efficiencies, and (d) power efficiencies.

tandem OLED fabrication utilizing printing or coating processes.

AUTHOR INFORMATION

Corresponding Authors

*E-mail: stefan.hoefle@kit.edu.
*E-mail: alexander.colsmann@kit.edu.

Author Contributions

$^{\nabla}$S.H. and C.B. contributed equally to this work.

Notes

The authors declare no competing financial interest.

ACKNOWLEDGMENTS

We thank Manuel Reinhard and Min Zhang for fruitful discussions. We acknowledge funding by the Federal Ministry of Education and Research under contract no. 13N12281 (projects PrintOLED and PrintOLED2). The authors thank the DFG Center for Functional Nanostructures (CFN) for support. S.H. thanks the Karlsruhe School of Optics & Photonics (KSOP) for support. A.C. acknowledges funding by the Federal Ministry of Education and Research under contract 03EK3504 (project TAURUS).

REFERENCES

(1) Pfeiffer, M.; Forrest, S. R.; Leo, K.; Thompson, M. E. Electrophosphorescent p−i−n Organic Light-Emitting Devices for Very-High-Efficiency Flat-Panel Displays. *Adv. Mater.* **2002**, *14*, 1633−1636.

(2) D'Andrade, B. W.; Forrest, S. R. White Organic Light-Emitting Devices for Solid-State Lighting. *Adv. Mater.* **2004**, *16*, 1585−1595.

(3) Sasabe, H.; Kido, J. Multifunctional Materials in High-Performance OLEDs: Challenges for Solid-State Lighting. *Chem. Mater.* **2011**, *23*, 621−630.

(4) Wu, H.; Zhou, G.; Zou, J.; Ho, C.-L.; Wong, W.-Y.; Yang, W.; Peng, J.; Cao, Y. Efficient Polymer White-Light-Emitting Devices for Solid-State Lighting. *Adv. Mater.* **2009**, *21*, 4181−4184.

(5) Sasabe, H.; Minamoto, K.; Pu, Y.-J.; Hirasawa, M.; Kido, J. Ultra High-Efficiency Multi-Photon Emission Blue Phosphorescent OLEDs with External Quantum Efficiency Exceeding 40%. *Org. Electron.* **2012**, *13*, 2615−2619.

(6) Sasabe, H.; Nakanishi, H.; Watanabe, Y.; Yano, S.; Hirasawa, M.; Pu, Y.-J.; Kido, J. Extremely Low Operating Voltage Green Phosphorescent Organic Light-Emitting Devices. *Adv. Funct. Mater.* **2013**, *23*, 5550−5555.

(7) Ishii, M.; Taga, Y. Influence of Temperature and Drive Current on Degradation Mechanisms in Organic Light-Emitting Diodes. *Appl. Phys. Lett.* **2002**, *80*, 3430−3432.

(8) Ke, L.; Chua, S.-J.; Zhang, K.; Yakovlev, N. Degradation and Failure of Organic Light-Emitting Devices. *Appl. Phys. Lett.* **2002**, *80*, 2195−2197.

(9) Hamwi, S.; Meyer, J.; Kröger, M.; Winkler, T.; Witte, M.; Riedl, T.; Kahn, A.; Kowalsky, W. The Role of Transition Metal Oxides in Charge-Generation Layers for Stacked Organic Light-Emitting Diodes. *Adv. Funct. Mater.* **2010**, *20*, 1762−1766.

(10) Tang, J.-X.; Fung, M.-K.; Lee, C.-S.; Lee, S.-T. Interface Studies of Intermediate Connectors and Their Roles in Tandem OLEDs. *J. Mater. Chem.* **2010**, *20*, 2539−2548.

(11) Hong, K.; Lee, J.-L. Charge Generation Mechanism of Metal Oxide Interconnection in Tandem Organic Light Emitting Diodes. *J. Phys. Chem. C* **2012**, *116*, 6427−6433.

(12) Pfeiffer, M.; Leo, K.; Zhou, X.; Huang, J.; Hofmann, M.; Werner, A.; Blochwitz-Nimoth, J. Doped Organic Semiconductors: Physics and Application in Light Emitting Diodes. *Org. Electron.* **2003**, *4*, 89−103.

DOI: 10.1021/acsami.5b00883
ACS Appl. Mater. Interfaces 2015, 7, 8132−8137

(13) Schwab, T.; Schubert, S.; Hofmann, S.; Fröbel, M.; Fuchs, C.; Thomschke, M.; Müller-Meskamp, L.; Leo, K.; Gather, M. C. Highly Efficient Color Stable Inverted White Top-Emitting OLEDs with Ultra-Thin Wetting Layer Top Electrodes. *Adv. Opt. Mater.* **2013**, *1*, 707−713.
(14) Kido, J.; Matsumoto, T.; Nakada, T. 27.1: Invited Paper: High Efficiency Organic EL Devices Having Charge Generation Layers. *SID Int. Symp. Dig. Technol. Pap.* **2003**, 964−965.
(15) Sun, J. X.; Zhu, X. L.; Peng, H. J.; Wong, M.; Kwok, H. S. Effective Intermediate Layers for Highly Efficient Stacked Organic Light-Emitting Devices. *Appl. Phys. Lett.* **2005**, *87*, 093504.
(16) Höfle, S.; Schienle, A.; Bernhard, C.; Bruns, M.; Lemmer, U.; Colsmann, A. Solution Processed, White Emitting Tandem Organic Light-Emitting Diodes with Inverted Device Architecture. *Adv. Mater.* **2014**, *26*, 5155−5159.
(17) Chiba, T.; Pu, Y.-J.; Sasabe, H.; Kido, J.; Yang, Y. Solution-Processed Organic Light-Emitting Devices with Two Polymer Light-Emitting Units Connected in Series by a Charge-Generation Layer. *J. Mater. Chem.* **2012**, *22*, 22769−22773.
(18) Talik, N. A.; Yeoh, K. H.; Ng, C. Y.; Yap, B. K.; Woon, K. L. Efficient Green Phosphorescent Tandem Organic Light Emitting Diodes with Solution Processable Mixed Hosts Charge Generating Layer. *J. Lumin.* **2014**, *154*, 345−349.
(19) Pu, Y.-J.; Chiba, T.; Ideta, K.; Takahashi, S.; Aizawa, N.; Hikichi, T.; Kido, J. Fabrication of Organic Light-Emitting Devices Comprising Stacked Light-Emitting Units by Solution-Based Processes. *Adv. Mater.* **2014**, *27*, 1327−1332.
(20) De Bruyn, P.; Moet, D. J. D.; Blom, P. W. M. A Facile Route to Inverted Polymer Solar Cells Using a Precursor Based Zinc Oxide Electron Transport Layer. *Org. Electron.* **2010**, *11*, 1419−1422.
(21) De Bruyn, P.; Moet, D. J. D.; Blom, P. W. M. All-Solution Processed Polymer Light-Emitting Diodes with Air Stable Metal-Oxide Electrodes. *Org. Electron.* **2012**, *13*, 1023−1030.
(22) Höfle, S.; Schienle, A.; Bruns, M.; Lemmer, U.; Colsmann, A. Enhanced Electron Injection into Inverted Polymer Light-Emitting Diodes by Combined Solution-Processed Zinc Oxide/Polyethylenimine Interlayers. *Adv. Mater.* **2014**, *26*, 2750−2754.
(23) Kim, Y.-H.; Han, T.-H.; Cho, H.; Min, S.-Y.; Lee, C.-L.; Lee, T.-W. Polyethylene Imine as an Ideal Interlayer for Highly Efficient Inverted Polymer Light-Emitting Diodes. *Adv. Funct. Mater.* **2014**, *24*, 3808−3814.
(24) Fukagawa, H.; Morii, K. Highly Efficient and Air-Stable Inverted Organic Light-Emitting Diode Composed of Inert Materials. *Appl. Phys. Express* **2014**, *7*, 082104.
(25) Murase, S.; Yang, Y. Solution Processed MoO_3 Interfacial Layer for Organic Photovoltaics Prepared by a Facile Synthesis Method. *Adv. Mater.* **2012**, *24*, 2459−2462.
(26) Tan, Z.; Qian, D.; Zhang, W.; Li, L.; Ding, Y.; Xu, Q.; Wang, F.; Li, Y. Efficient and Stable Polymer Solar Cells with Solution-Processed Molybdenum Oxide Interfacial Layer. *J. Mater. Chem. A* **2013**, *1*, 657−664.
(27) Choi, H.; Kim, B.; Ko, M. J.; Lee, D.-K.; Kim, H.; Kim, S. H.; Kim, K. Solution Processed WO_3 Layer for the Replacement of PEDOT:PSS Layer in Organic Photovoltaic Cells. *Org. Electron.* **2012**, *13*, 959−968.
(28) Tan, Z.; Li, L.; Cui, C.; Ding, Y.; Xu, Q.; Li, S.; Qian, D.; Li, Y. Solution-Processed Tungsten Oxide as an Effective Anode Buffer Layer for High-Performance Polymer Solar Cells. *J. Phys. Chem. C* **2012**, *116*, 18626−18632.
(29) Meyer, J.; Hamwi, S.; Kröger, M.; Kowalsky, W.; Riedl, T.; Kahn, A. Transition Metal Oxides for Organic Electronics: Energetics, Device Physics and Applications. *Adv. Mater.* **2012**, *24*, 5408−5427.
(30) Huang, J.-S.; Chou, C.-Y.; Liu, M.-Y.; Tsai, K.-H.; Lin, W.-H.; Lin, C.-F. Solution-Processed Vanadium Oxide as an Anode Interlayer for Inverted Polymer Solar Cells Hybridized with ZnO Nanorods. *Org. Electron.* **2009**, *10*, 1060−1065.
(31) Zilberberg, K.; Meyer, J.; Riedl, T. Solution Processed Metal-Oxides for Organic Electronic Devices. *J. Mater. Chem. C* **2013**, *1*, 4796−4815.
(32) Zilberberg, K.; Trost, S.; Schmidt, H.; Riedl, T. Solution Processed Vanadium Pentoxide as Charge Extraction Layer for Organic Solar Cells. *Adv. Energy Mater.* **2011**, *1*, 377−381.
(33) Chen, C.-P.; Chen, Y.-D.; Chuang, S.-C. High-Performance and Highly Durable Inverted Organic Photovoltaics Embedding Solution-Processable Vanadium Oxides as an Interfacial Hole-Transporting Layer. *Adv. Mater.* **2011**, *23*, 3859−3863.
(34) Höfle, S.; Do, H.; Mankel, E.; Pfaff, M.; Zhang, Z.; Bahro, D.; Mayer, T.; Jaegermann, W.; Gerthsen, D.; Feldmann, C.; Lemmer, U.; Colsmann, A. Molybdenum Oxide Anode Buffer Layers for Solution Processed, Blue Phosphorescent Small Molecule Organic Light Emitting Diodes. *Org. Electron.* **2013**, *14*, 1820−1824.
(35) Höfle, S.; Bruns, M.; Strässle, S.; Feldmann, C.; Lemmer, U.; Colsmann, A. Tungsten Oxide Buffer Layers Fabricated in an Inert Sol-Gel Process at Room-Temperature for Blue Organic Light-Emitting Diodes. *Adv. Mater.* **2013**, *25*, 4113−4116.
(36) Köhnen, A.; Irion, M.; Gather, M. C.; Rehmann, N.; Zacharias, P.; Meerholz, K. Highly Color-Stable Solution-Processed Multilayer WOLEDs for Lighting Application. *J. Mater. Chem.* **2010**, *20*, 3301−3306.
(37) Zhou, Y.; Fuentes-Hernandez, C.; Shim, J.; Meyer, J.; Giordano, A. J.; Li, H.; Winget, P.; Papadopoulos, T.; Cheun, H.; Kim, J.; Fenoll, M.; Dindar, A.; Haske, W.; Najafabadi, E.; Khan, T. M.; Sojoudi, H.; Barlow, S.; Graham, S.; Brédas, J.-L.; Marder, S. R.; Kahn, A.; Kippelen, B. A Universal Method to Produce Low-Work Function Electrodes for Organic Electronics. *Science* **2012**, *336*, 327−332.
(38) Reinhard, M.; Eckstein, R.; Slobodskyy, A.; Lemmer, U.; Colsmann, A. Solution-Processed Polymer−Silver Nanowire Top Electrodes for Inverted Semi-Transparent Solar Cells. *Org. Electron.* **2013**, *14*, 273−277.
(39) Qi, X.; Li, N.; Forrest, S. R. Analysis of Metal-Oxide-Based Charge Generation Layers Used in Stacked Organic Light-Emitting Diodes. *J. Appl. Phys.* **2010**, *107*, 014514.

DOI: 10.1021/acsami.5b00883
ACS Appl. Mater. Interfaces 2015, 7, 8132−8137